Chapter 5

Effect of different rare earths (Samarium, Dysprosium, Terbium) doping on the emission characteristics of the Sr_2CeO_4 phosphor

5.1 Introduction.

In the last chapter we discussed the possible energy transfer mechanism occurring in the Sr_2CeO_4 doped with europium phosphor. Also the effect of the particle size with respect to two different synthesis techniques has been observed and discussed in the length. In this chapter we elaborate the energy transfer mechanism of the Sr_2CeO_4 phosphor by doping them with various rare earths. The main aim in this chapter is to study the emission of white light from the rare earth doped phosphor, synthesized by sol-gel technique and the possible energy transfer mechanism.

The nanoscale rare earth doped phosphors is the most exciting field, attracting attention of the scientists and researchers all over the world. There is a large number of literature available on the effect of the particle size on the luminescence characteristics of the europium doped phosphor but still there are no reports on the effect of samarium, dysprosium and terbium doping in the Sr_2CeO_4. It is well known that the charge transfer (CT) transition is sensitive to ligand environment i.e. the potential field of the ligands. In order to find out how the next-nearest-neighbour (NNN) of the central metal ion (Ce^{4+}, in this case) affects the Ce^{4+}-O^{2-} CT transition, Sr_2CeO_4 has been doped with different rare-earth ions e.g. Dy^{3+}, Sm^{3+} or Tb^{3+}. These ions have unique CT associated excited states in their complexes with halogen ligands or in oxides.

The interconfigurational $4f^n$ to $4f^{n-1}5d$ transitions of the rare-earth ions have become increasingly important in recent years because of their applications in fast scintillators and ultraviolet laser sources. The $4f^n$ to $4f^{n-1}5d$ transitions involve the transfer of a single electron from the 4f shell to the empty 5d shell of the ion, and are therefore sometimes simply referred to as 4f to 5d transitions. These transitions are parity allowed (Laporte's selection rule) with oscillator strengths ranging from 10^{-6} to values approaching 0.1 in some cases; this is up to 10,000 times stronger than the strongest $4f^N$ to $4f^N$ transitions, which are parity forbidden. Unlike the shielded intraconfigurational $4f^N$ to $4f^N$ transitions, the 4f to 5d transitions are strongly affected by the host lattice. This arises since the 5d electron is the outermost electron of the ion and mixes significantly with the electronic states of its neighboring ions so that the environment is the dominant effect on the 5d energy level structure. The $4f^{n-1}5d$ levels exhibit electronic

structure corresponding to the large crystal field splitting of the 5d levels coupled to the splittings of the $4f^{n-1}$ electronic core. Interactions between the localized 4f electronic states of rare earth ions and the de-localized band states of the crystal lattice can strongly affect the optical properties of technologically important rare-earth-doped materials. In contrast to the well-developed understanding of the electronic structure of the $4f^n$ states, relatively little is known about the relationships between these states and the electronic states of the crystal **[1, 2]**. In recent years, the body of knowledge on this topic has steadily grown due to the strong interest in developing more efficient phosphor. The performance of rare-earth-activated optical materials in these applications can be enhanced, reduced, or even entirely inhibited by energy exchange and charge transfer processes between the rare earth ions and the host crystal. This has made it increasingly important that the systematic trends and behavior of rare earth energies relative to crystal band states be explored and characterized.

Samarium in trivalent form is an ion that shows the lasing property in TbF_3 and is used as a commercial phosphor in $CaWO_4$ **[3, 4]**. It has also been used for down conversion of $ZrO_2:Sm^{3+}$ nanophosphor **[5]**. The material Sr_2CeO_4 has been synthesized by various methods in the recent years after the discovery of the same by combinatorial synthesis by Danielson et al **[6]**. The sol-gel method offers several advantages over the conventional solid state reaction route and other techniques **[7]**. However the purity of the host matrix and the homogeneity of the activators are very important criteria for making efficient phosphors. The surface area of the powders produced from the sol-gel is very high leading to lowering of processing temperature and time. In this regard, $Sr_2CeO_4:Ln^{3+}$(Sm, Dy, Tb) can also act as an efficient white light emitter considering their property of emitting sharp emission in the visible region. In the present work, we illustrate an interesting approach to understand the mechanism of energy transfer from Sr_2CeO_4 (sensitizer) host to the dopants (activator) by incorporating the rare-earth ions (Sm^{3+}, Dy^{3+} and Tb^{4+}) which have unique charge-transfer associated excited states in their complexes with halogen ligands or in oxides. The detailed feature of the excitation and emission properties of Sm^{3+} or Dy^{3+} doped Sr_2CeO_4 is clearly demonstrated, leading to an explanation for an energy transfer mechanism between the absorbing host and the rare-earth emitters. Till date there are no reports on the doping of samarium, dysprosium and terbium in the Sr_2CeO_4 using

sol-gel method and only two reports, one by Nag et al [8] and one by Xianghong et al [9] by wet chemical and co-precipitation respectively. Our main aim was to study the effect of all the above trivalent rare earth elements in it and to study the radiative transitions taking place.

5.2 Experimental

The synthesis route (Sol-gel) adopted by us has already been discussed in detail in chapter three. The Strontium and Cerium nitrates were taken in the 2:1 ratio along with an appropriate doping of Samarium, Dysprosium and Terbium. The powders were taken according to the nominal composition of $Sr_{1-x/2}(NO_3)_2$ + $Ce(NO_3)_3.9H_2O$+$xSm(NO_3)_3$ (where x = 0.03125%, 0.125%, 0.25%, 0.5%, 1%, 1.5%, 2%). For the Dysprosium and Terbium, the doping was done with 0.5mol%, 1.0mol% and 1.5mol% and for easiness are given in table-1. All the above were dissolved in distilled water and kept for stirring. Ethylene glycol and citric acid were added at an appropriate time and the heating was raised to 80-90°C at constant stirring. The material transformed into a yellowish gel, which was then kept for drying in an oven at 100°C for 4 hrs. The dried powder was fired in furnace at 1200°C for 2 hrs in air and was subjected to various characterization processes. Few samples were also fired at different temperatures 400 and 800°C for 2 hrs to see the effect of heating on the crystallanity of the synthesized compound.

The reaction can be described as:

$$2Sr_{1-x/2}(NO_3)_2+Ce(NO_3)_3.9H_2O+xLn(NO_3)_3 \rightarrow Sr_{2-x}CeO_4:xLn^{3+}\ (Sm, Dy, Tb)$$

Sr. No.	Sample Name	Mole Percentage
1	$Sr_2CeO_4:Sm^{3+}$	0.03125, 0.125, 0.25, 0.5, 1.0, 1.5, 2.0
2	$Sr_2CeO_4:Dy^{3+}$	0.5, 1.0, 1.5
3	$Sr_2CeO_4:Tb^{3+}$	0.5, 1.0, 1.5

Table -1 Different rare earth dopant concentrations along with the host.

5.3.1 Characterization

5.3.1(a) X-ray Diffraction studies

Phase identification of the powders was carried out by the X-ray powder diffraction technique using RIGAKU D'MAX III Diffractometer having Cu Kα radiation (λ = 0.154nm). The scan range was kept from 5 degrees to 80 degrees at the scan speed of 0.05 degree per second. Details are given in chapter two.

5.3.1(b) Scanning Electron microscope (SEM)

The Scanning Electron Micrograph images (SEM) of the samples were taken using JEOL make JSM-5610 LV for studying the morphology of the compound, details in chapter two.

5.3.1(c) Photoluminescence measurements

The photoluminescence (Emission and Excitation spectra) were recorded at room temperature using spectrofluorophotometer RF-5301 PC of SHIMADZU make, details in chapter two. The source used in this is a xenon lamp. The slit width for the emission and excitation was kept at 1.5nm for all the measurements. A filter was used to remove the second order peak of the excitation light in the PL measurements. The sensitivity of the instrument was set as high unless stated otherwise.

5.3.1(d) Commission Internationale de l'Eclairage (CIE) coordinates

For the present study, the *Equidistant-Wavelength method* has been used to determine the coordinates on the colorimetric chromaticity diagram. The CIE coordinates for the samples have been calculated for CIE 1931, CIE 1960 and CIE 1976, details have been given in chapter two.

5.4 Result and Discussion

5.4.1 X-ray diffraction studies

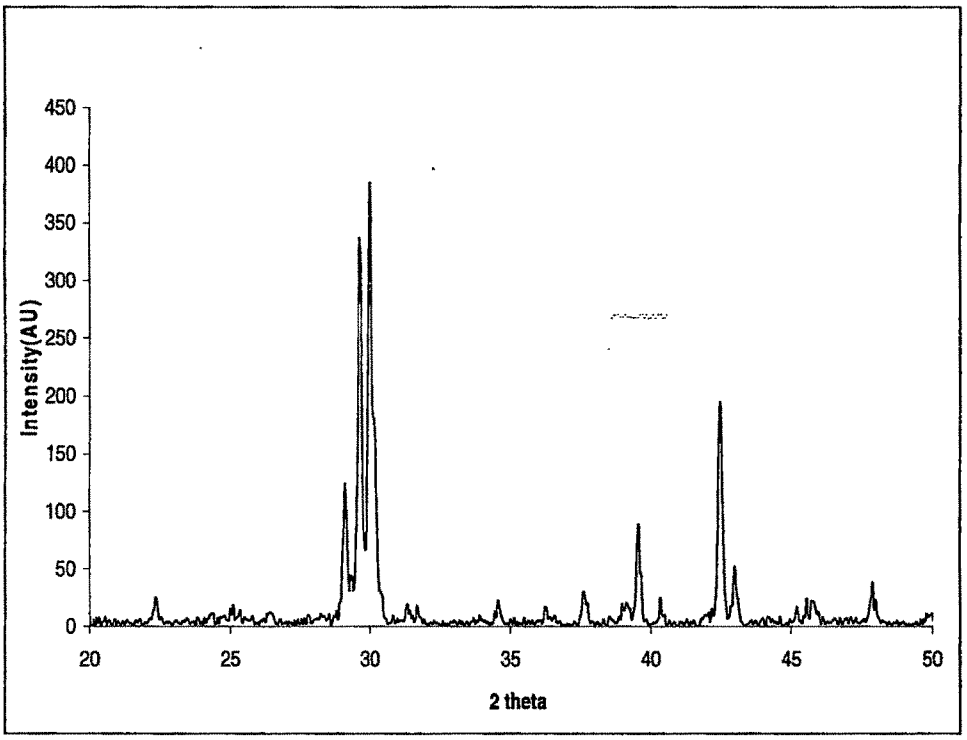

Figure-1 The X-ray Diffraction pattern of the sample Sr_2CeO_4 doped with 0.1mol% of samarium.

The figure-1 shows the powder X-ray diffraction pattern of the synthesized phosphor sample. The result shows that the phase of the material is almost pure with traces of $SrCeO_3$ present in it a bit. The average crystallite size was calculated using the Scherrer formula

$$d = \frac{k\lambda}{\beta \cos \theta_B},$$

Where k = Constant (0.9), λ = Wavelength of the x-ray (0.154 nm in the present case), β = full width at half-maxima (FWHM), θ = Bragg angle of the XRD peak. The crystallinity of the compound as revealed by the XRD pattern, increased on raising the calcining temperature. This was also observed by Shikao Shi et al. **[10]**. From the analysis of the XRD pattern, it was understood that the introduction of activator (Ln^{3+}) did not influence the crystal structure of the phosphor matrix. The calculated average crystal size of the sample calculated by

measuring the full width half maxima was found to be of about 55nm for Samarium (1.0mol %) doped sample.

5.4.2 Scanning electron microscopy (SEM)

The scanning electron micrograph of the Sr_2CeO_4 phosphor doped with samarium (1.0mol%) have been presented in figure below.

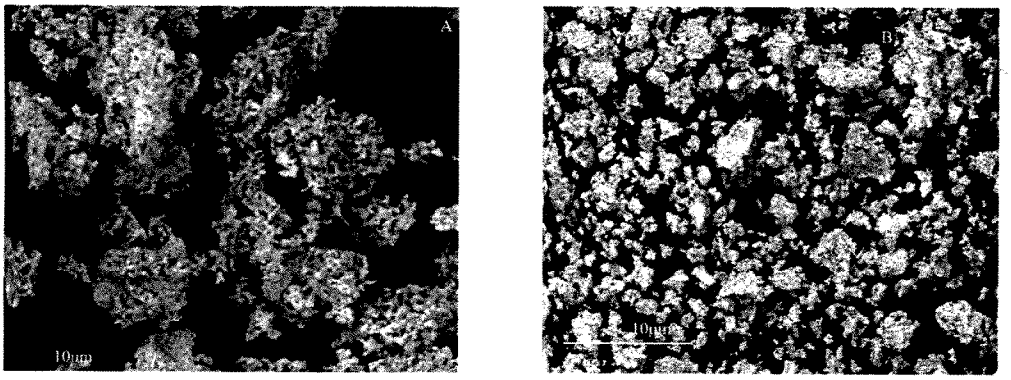

A. Sol-Gel synthesized (800°C)

B. Sol-Gel synthesized (1200°C)

Micrographs of the Sol-Gel synthesized $Sr_2CeO_4:Sm^{3+}$(1.0mol%) heated at different temperatures.

From the Scanning electron micrographs, it is observed that the sample prepared via sol-gel route has rod like shape with a network attached to each other. At higher temperatures it appears that the particles have agglomerated and resulted in growth.

5.4.3 Photoluminescence Spectra

5.4.3(a) Luminescence of Samarium doped Sr_2CeO_4

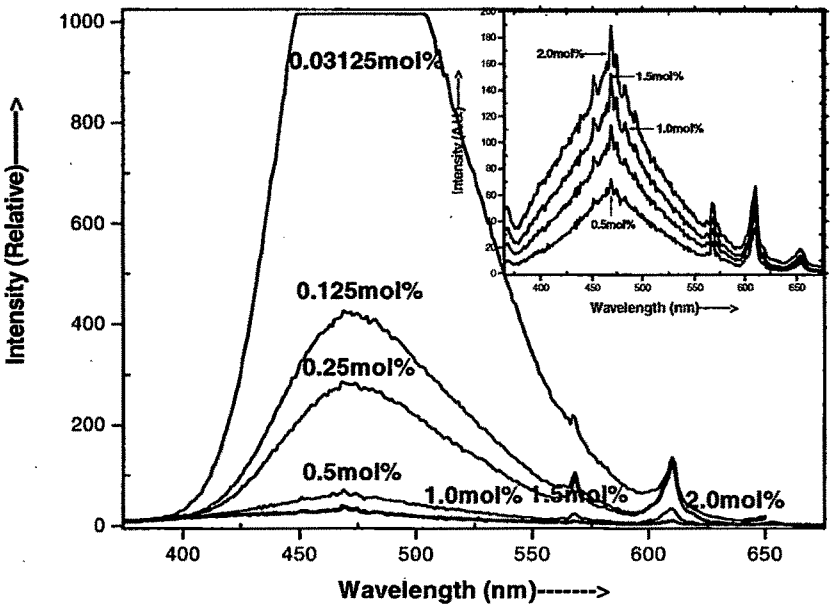

Figure-2 **The Photoluminescence emission spectra of the $Sr_2CeO_4:Sm^{3+}$ at 254nm excitation.**

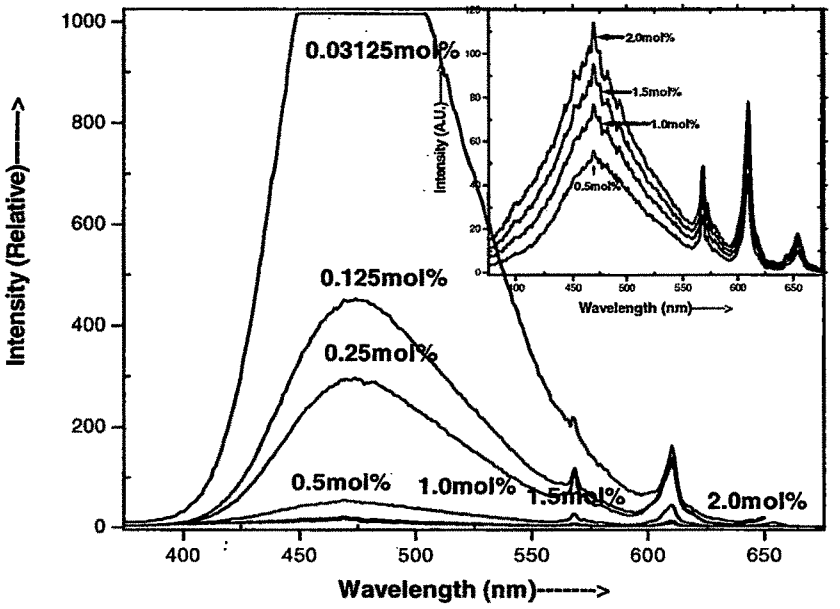

Figure-3 **The Photoluminescence emission spectra of the $Sr_2CeO_4:Sm^{3+}$ at 280nm excitation.**

Sr. No.	Sample Name	Percentage of Samarium
1	Sr_2CeO_4 Curve B	0.03125
2	Sr_2CeO_4 Curve C	0.125
3	Sr_2CeO_4 Curve E	0.25
4	Sr_2CeO_4 Curve F	0.5
5	Sr_2CeO_4 Curve G	1.0
6	Sr_2CeO_4 Curve H	1.5
7	Sr_2CeO_4 Curve I	2.0

Table-2 Percentage of samarium doping in the Sr_2CeO_4 sample.

To study the effect of trivalent samarium doping and to see the effect of the same on the emission characteristics of the host, photoluminescence spectra were recorded at room temperature for the $Sr_2CeO_4:Sm^{3+}$ (0.03125%, 0.125%, 0.25%, 0.5%, 1%, 1.5%, 2%) and are shown in figure-2 and 3 under 254nm and 280nm excitation respectively. The table-2 gives a detailed description of the graph plotted. Upon excitation with 254nm wavelength the emission spectra shows the broad Ce^{4+}-O^{2-} charge transfer band in the blue region superimposed with the Sm^{3+} emission lines in the yellow and red region. These spectral features are characteristic of intraconfigurational f-f transitions of the RE ions. Because tetravalent cerium in Sr_2CeO_4 has no 4f electrons, emissions are due to the presence of Sm^{3+} having five 4f electrons. For lower concentration of samarium, the emission is out of range for the Ce^{4+}-O^{2-} charge transfer transitions of the sample and the samarium peaks appear very weak. But on increasing the samarium concentration the sharp lines of the samarium emission appear prominently and the Ce^{4+}-O^{2-} CT transitions of the host decreases relatively. The narrow lines are assigned to the transitions from the between $^4G_{5/2}$ excited state to the lower ^6H_J (J = 5/2, 7/2 and 9/2) energy levels of the ground multiplets of Sm^{3+}. This is in contrast to the emission observed in the $CeO_2:Sm^{3+}$[**11-13**] but match with those observed for materials with lower symmetry such as monoclinic ZrO_2 [**14**]. According to the selection rules, [**1**] magnetic dipole transitions that obey J = 0 and ±1 (J = total angular momentum) are allowed for Sm^{3+} in a site with inversion symmetry. The emission spectra for the Sr_2CeO_4 sample were peaking at the 469nm but when doped with samarium, the emission spectra are dominated by the red $^4G_{5/2}\rightarrow{}^6H_{7/2}$ transition centered at 610nm. Additional

emissions were observed at the 567 and 654nm ascribed to the $^4G_{5/2} \rightarrow {}^6H_{5/2}$ and $^4G_{5/2} \rightarrow {}^6H_{9/2}$ transitions, respectively. The corresponding energy along with the transitions have been shown in table-3.

Wavelength (nm)	Transitions	Energy (eV)	Energy (cm^{-1})
410	$^6H_{5/2} \rightarrow {}^6P_{3/2}$	3.02	24390
429	$^6H_{5/2} \rightarrow {}^6P_{5/2}$	2.89	23310
567	$^4G_{5/2} \rightarrow {}^6H_{5/2}$	2.18	17636
610	$^4G_{5/2} \rightarrow {}^6H_{7/2}$	2.03	16393
654	$^4G_{5/2} \rightarrow {}^6H_{9/2}$	1.89	15290

Table-3 The different energy transitions of the samarium in the host Sr_2CeO_4.

The emission spectra shows broad Ce^{4+}-O^{2-} CT emission band in the blue-green region superimposed with the Sm^{3+} emission lines in the yellow and orange-red regions. It is further observed from the emission spectra of Sr_2CeO_4:Sm (0.03125% to 2%), that as the samarium concentration increases, the photoluminescence intensity at 469nm goes on decreasing but the intensity at 567nm and 610nm shows an increase for Samarium (0.25mol%) concentrations. The percentage decrease in the intensity for the 472nm peak is 56% for 0.125mol% and 71% for the 0.25mol%, whereas for the 567nm peak the percentage fall is 49% for 0.125mol% and 54% for the 0.25mol% but for the 610nm peak the increase at first is for 11% for the 0.125mol% and an increase of 30% for the 0.25mol%. The intensity reaches its maxima at 610nm for the Samarium concentration of 0.25%. There is a strong concentration dependence of the samarium on the emission spectrum of the Sr_2CeO_4, this is due to the nanocrystallite size of the host, such concentration dependence was also observed by Vetrone et al [**15**]. The emission spectra of the Sr_2CeO_4 sample doped with samarium has been shown in the figure-2 when excited with 280nm wavelength. This is almost same as for the excitation with 254nm, with difference being only in the intensity, the appearance of the samarium peaks at same wavelengths as with 254nm.

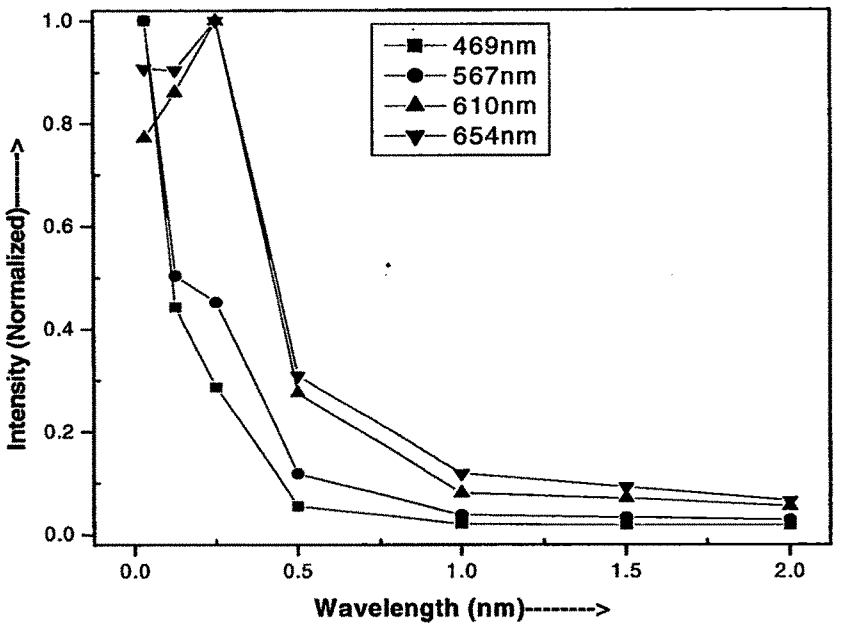

Figure-4 Variation of Intensity at different wavelengths with the concentration of samarium.

The photoluminescence intensity variation with the change in concentration of samarium has been shown in figure-4 (The intensity have been normalized for better viewing). Observed from the graph is that the intensity of the peaks at all wavelengths i.e. 469, 567, 610 and 654nm respectively, have high intensity at the lower concentration of samarium. Increasing the concentration of samarium up to 0.25mol% increases the intensity of the peaks at 610nm and 654nm but there is gradual fall in the intensity of 469 and 567nm. Thereon there is a gradual fall in the intensity for the higher concentration (<0.5mol%) and it saturates from 1.0mol% onwards. This is clearly the concentration quenching effect observed in the samarium doped Sr_2CeO_4. We may conclude that the quenching of the samarium in Sr_2CeO_4 is ~0.25mol%. This was not observed by Nag et al **[8]** but we are at variance with them on this result, and we may conclude that this may be due to the formation of nanosize of the Sr_2CeO_4 doped with samarium. Moreover we know that the concentration quenching increases for the nanocrystal as they can accommodate more particles **[16]**.

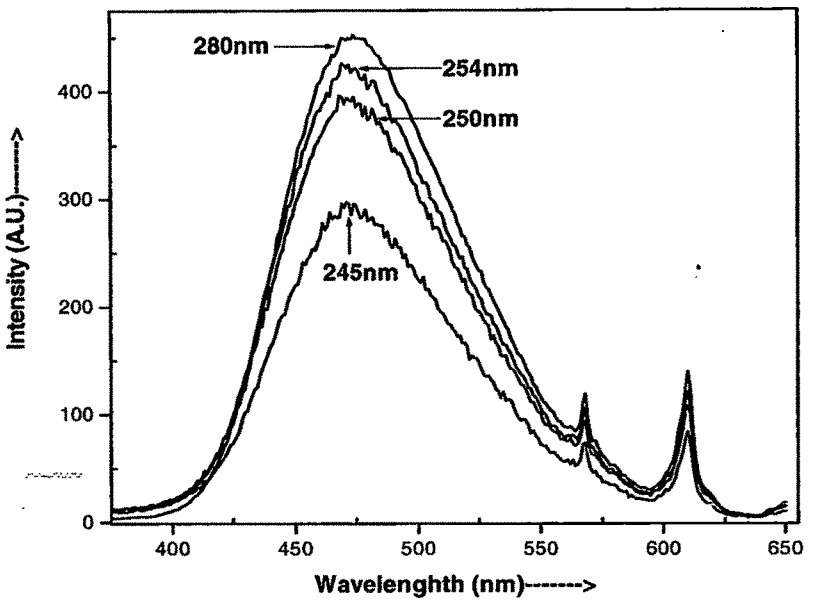

Figure-5 The photoluminescence emission spectra of the $Sr_2CeO_4:Sm^{3+}$(0.125mol%) under different excitation.

Figure-5 is the emission spectra of samarium 0.125mol% doped Sr_2CeO_4 with different excitation at 245, 250, 254 and 280nm. It is observed that the intensity of the 280nm is highest followed by 254nm but there is appearance of all the samarium transitions and the CT transitions simultaneously. This also shows that the vast range of excitation was able to excite the host as well as the samarium transitions. As all the different concentrations of samarium doped samples showed the same patterns so the graphs for all are not shown.

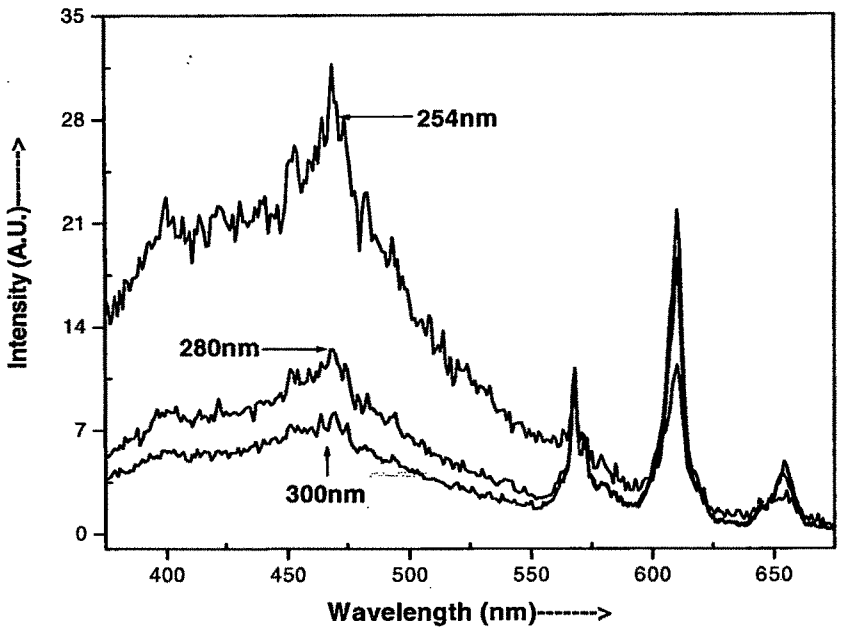

Figure-6A Photoluminescence emission spectra of the $Sr_2CeO_4:Sm^{3+}$(0.03125mol%) under different excitation (Heated at 400°C).

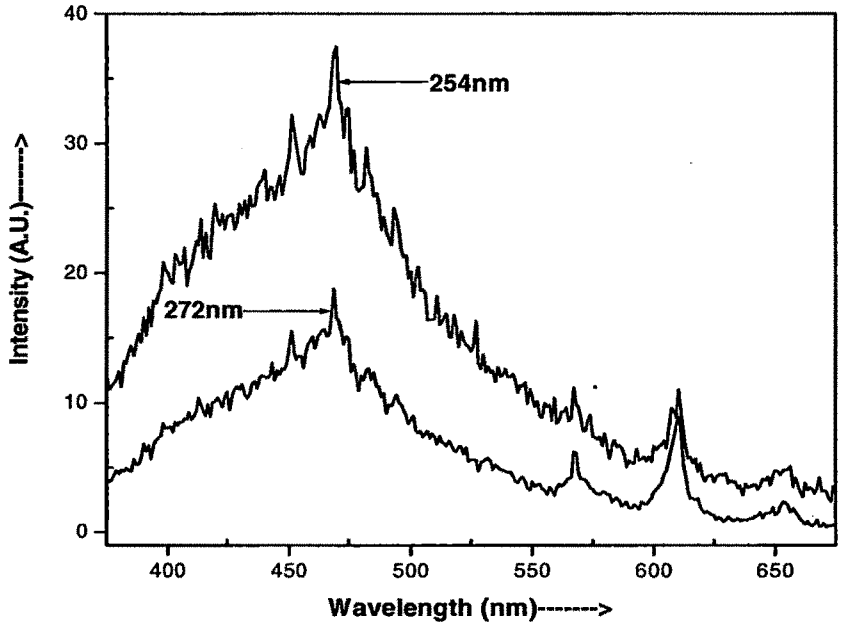

Figure-6B Photoluminescence emission spectra of the $Sr_2CeO_4:Sm^{3+}$(0.03125mol%) under different excitation (Heated at 800°C).

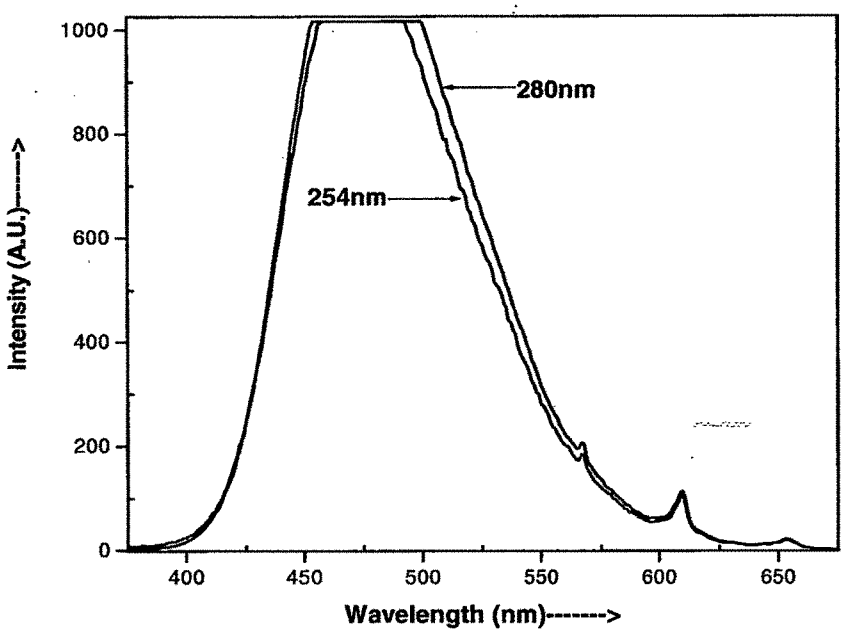

Figure-6C Photoluminescence emission spectra of the $Sr_2CeO_4:Sm^{3+}$(0.03125mol%) under different excitation (Heated at 1200°C).

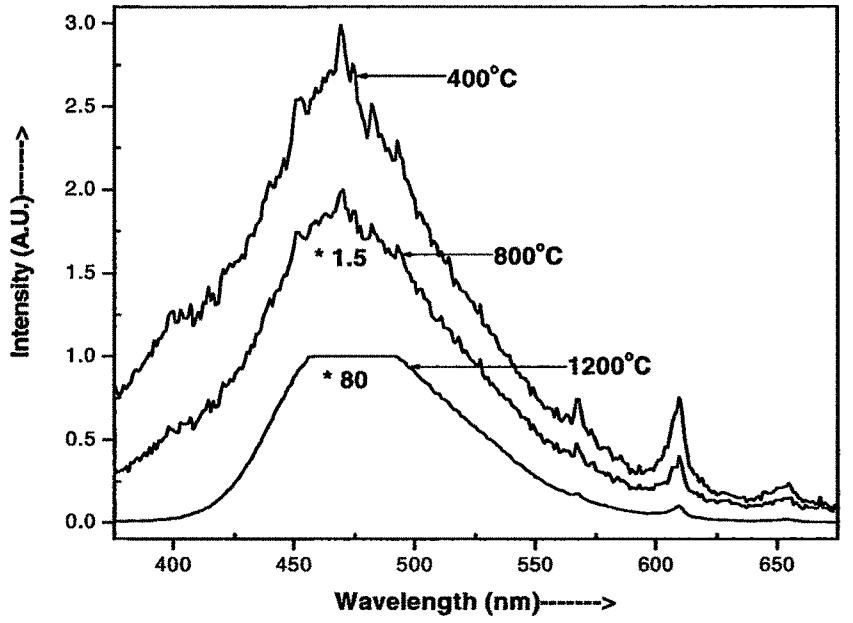

Figure-6D Photoluminescence emission spectra of the $Sr_2CeO_4:Sm^{3+}$(0.03125mol%) under 254nm excitation heated at different temperatures.

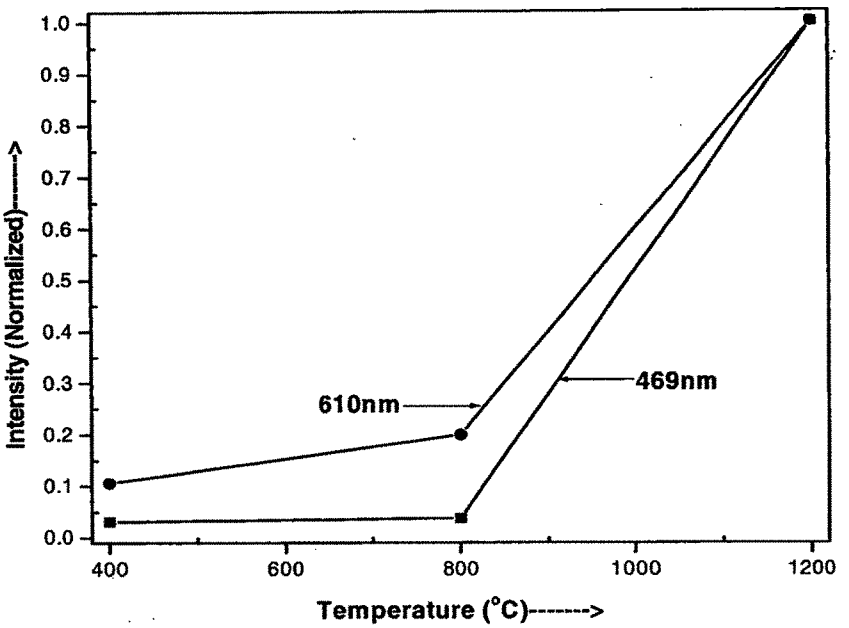

Figure-6E Variation of temperature with intensity at different wavelengths.

Figure-6 A, B and C are for the sample heated at different temperatures i.e. at 400, 800 and 1200°C respectively for samarium (0.03125mol%) doped Sr_2CeO_4. The interesting observation here is that as the temperature is raised from 400 to 1200°C, the crystallanity of the sample increases with an increment in intensity. The charge transfer transition at 1200°C became out of range along with the appearance of $^4G_{5/2} \rightarrow {}^6H_J$ (J = 5/2, 7/2 and 9/2) samarium transitions. Figure 6D shows the emission spectra at 254nm excitation for the samples heated at different temperatures (the figure marked inside are the intensity multiplication w.r.t. 400°C). Figure-6E shows the effect of heating at different temperatures and elucidate the conclusion that we draw regarding the crystallanity of the sample as also discussed in detail in chapter three. The crystallanity of the sample increases with a sharp increase in the photoluminescence intensity.

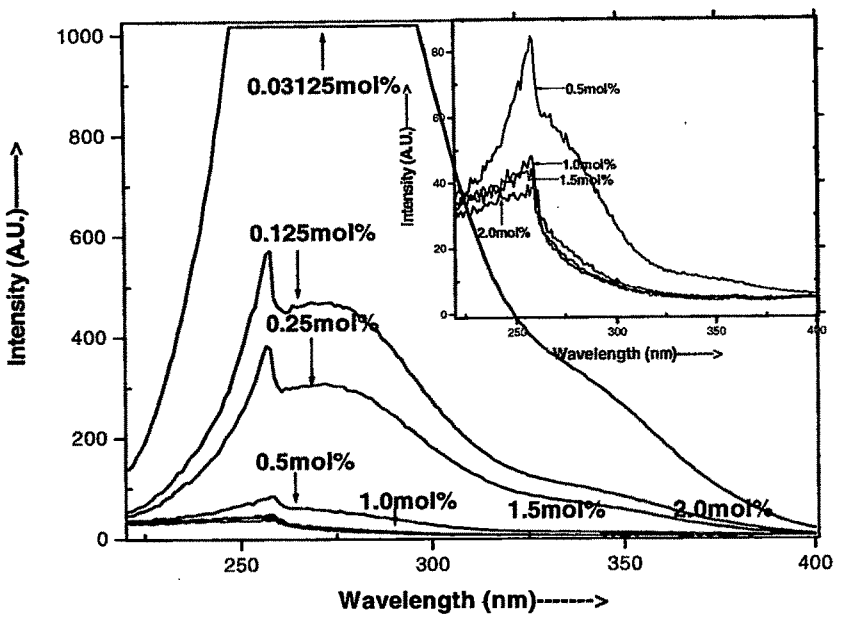

Figure-7 Photoluminescence excitation spectra of the $Sr_2CeO_4:Sm^{3+}$ monitored with 472nm excitation. (Inset is the excitation spectra of the higher mol% shown for clarity)

The excitation spectra of the $Sr_2CeO_4:Sm^{3+}$ doped phosphor for all the concentrations are shown in figure-7 monitored at 472nm. The peak around 259nm was observed along with humps at 272nm and 342nm. Interesting thing here to note is the disappearance of the hump at 272nm as the concentration of the samarium was increased; from 1.0mol% onwards the hump disappears. Moreover at the lowest (0.03125mol%) concentration of samarium, the intensity was out of range from 248nm to 297nm. The broad band is assigned to the Ce^{4+}-O^{2-} charge transfer excitation band whereas the hump at 342nm may be due to the trivalent samarium excitation transition. It was also observed that the Ce^{4+}-O^{2-} charge transfer band remains the most intense even for the highest concentration of samarium doped samples.

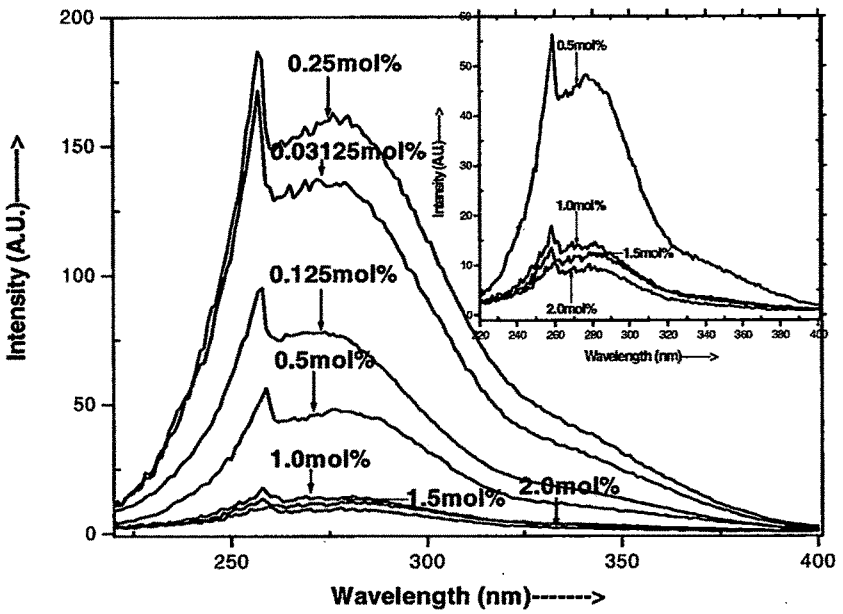

Figure-8 Photoluminescence excitation spectra of the $Sr_2CeO_4:Sm^{3+}$ monitored with 610nm excitation. (Inset is the excitation spectra of the higher mol% shown for clarity).

The excitation spectra of the $Sr_2CeO_4:Sm^{3+}$ doped phosphor for all the concentrations are shown in figure-8 monitored with the 610nm. The emission pattern is also similar to that when monitored with 472nm but here we observe that the intensity of the 0.25mol% doped sample is highest followed by 0.03125mol% and the rest. This is in correlation with the emission for the same. Another interesting point noticed here is that the intensity is not out of range for any sample. Moreover there is no disappearance of the hump at 270nm, for the sample when monitored with 472nm wavelength, even at high concentrations of samarium and the peak shape remains unchanged.

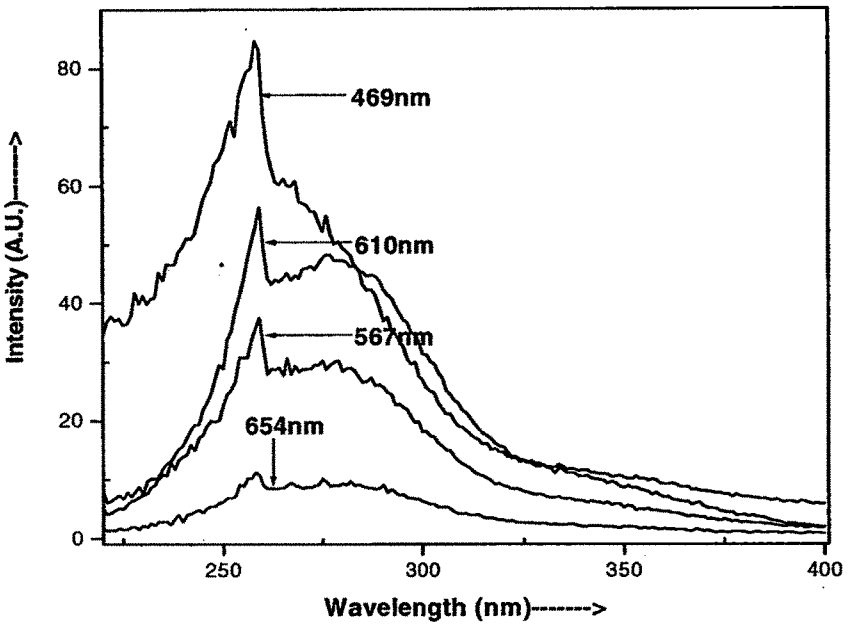

Figure-9 Photoluminescence excitation spectra of the $Sr_2CeO_4:Sm^{3+}$ (0.5mol%) monitored at different wavelengths.

Figure-9 is the excitation spectra of the 0.5mol% samarium doped Sr_2CeO_4 monitored at different wavelengths. We observe that the peak intensity is highest for the 469nm monitored wavelength followed by 610, 567 and 654nm respectively. One more important observation is the shape of the excitation peak is a bit different for the 469nm monitored sample, the hump at ~270nm has a steep fall compared to the others, all the other follow similar shape and the same pattern. This shows that the emission of the CT transition band along with samarium excitation band appears for the 567, 610 and 654nm respectively but not for the 467nm as this is the emission for the host Sr_2CeO_4. The samarium emission is due to the $^4G_{5/2} \rightarrow {}^6H_J$ (where J = 5/2, 7/2 and 9/2).

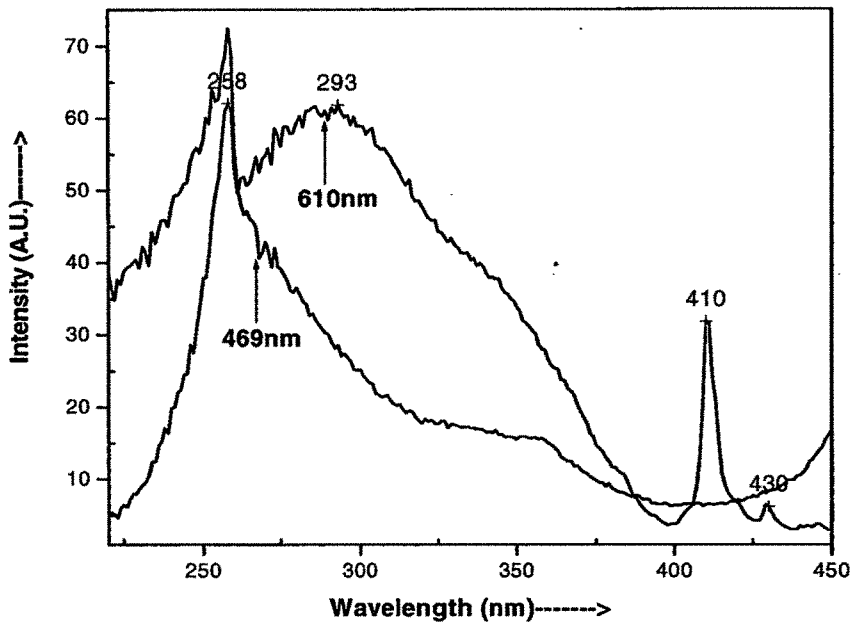

Figure-10 Photoluminescence excitation spectra of the $Sr_2CeO_4:Sm^{3+}$ (1.0mol%) monitored at different wavelengths.

Figure-10 is the excitation spectra of the 1.0mol% samarium doped Sr_2CeO_4 monitored at 469 and 610nm wavelengths as the 469nm coincides with the host emission and 610nm being the most intense peak for the samarium doped host. The additional peaks that appear in this are $^6H_{5/2}$ level to $^6P_{3/2}$ and $^6P_{5/2}$ excited states of Samarium in trivalent state. An interesting observation is the nature of the excitation pattern for both, we observe that for the 469nm wavelength the additional peaks are not observed as these are characteristics trivalent samarium excitation peak and they appear only when monitored with 610nm. This clearly differentiates the excitation pattern for both, showing the presence of two centers from which the excitation takes place. This was not observed for the others implying that there are two types.

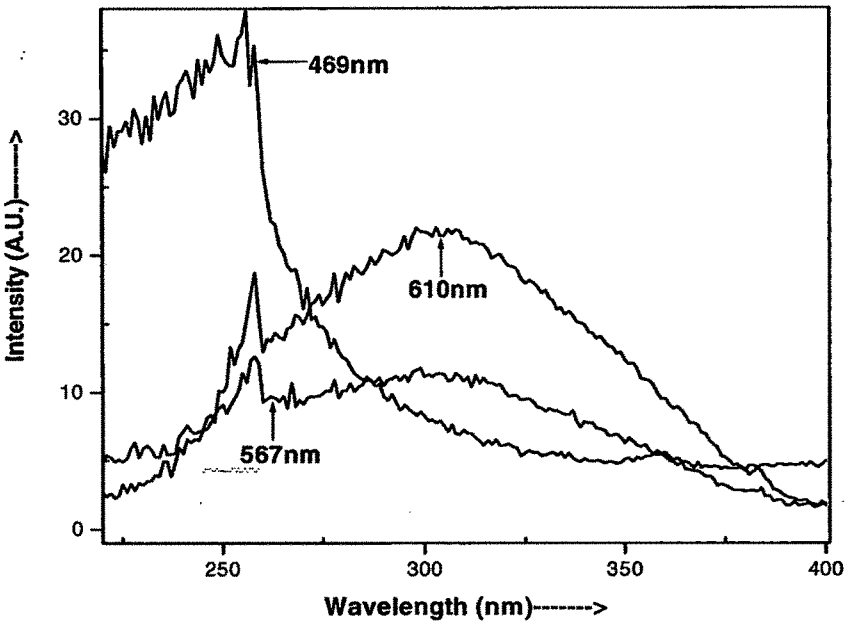

Figure-11 Photoluminescence excitation spectra of the $Sr_2CeO_4:Sm^{3+}$ (2.0mol%) monitored at different wavelengths.

Figure-11 is the excitation spectra of the 2.0mol% doped samarium peak when monitored with 469, 567 and 610nm respectively. In this also there is a clear distinction between the 469nm monitored and the 567 and 610nm monitored peak. As the concentration of samarium in the host is increased, there is a remarkable increase in the excitation at around ~300nm and the host maxima (sharp line) at 254nm decreases, this enhancement in the intensity at ~300nm is due to the presence of the trivalent samarium in the host and it correlates to the emission spectra at the same mol%. This shows that at higher concentration of samarium in the host, the excitation due to the samarium ions get enhanced and due to the host gets suppressed.

5.4.3 (b) Luminescence of Dysprosium and Terbium

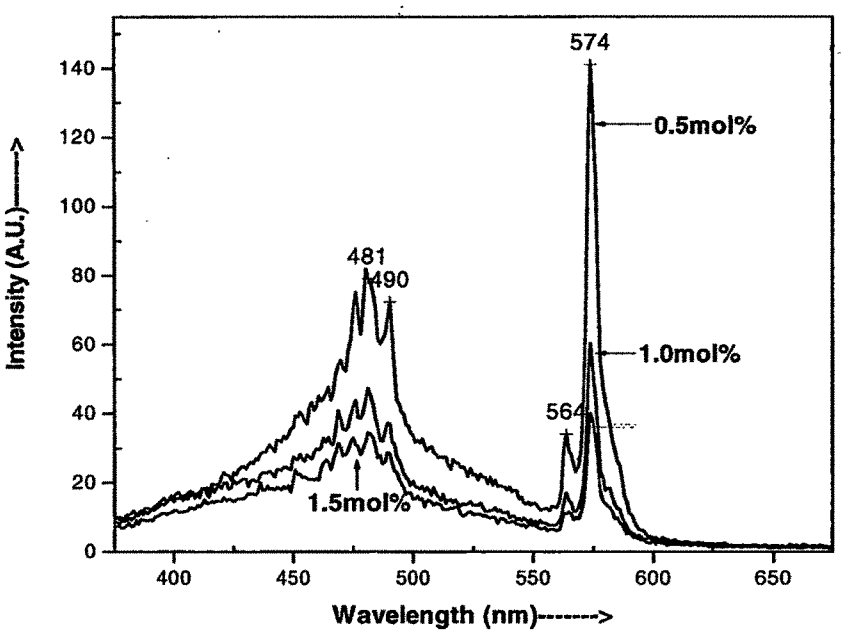

Figure-12 Photoluminescence emission spectra of the $Sr_2CeO_4:Dy^{3+}$ excited at 254nm wavelength for all concentrations.

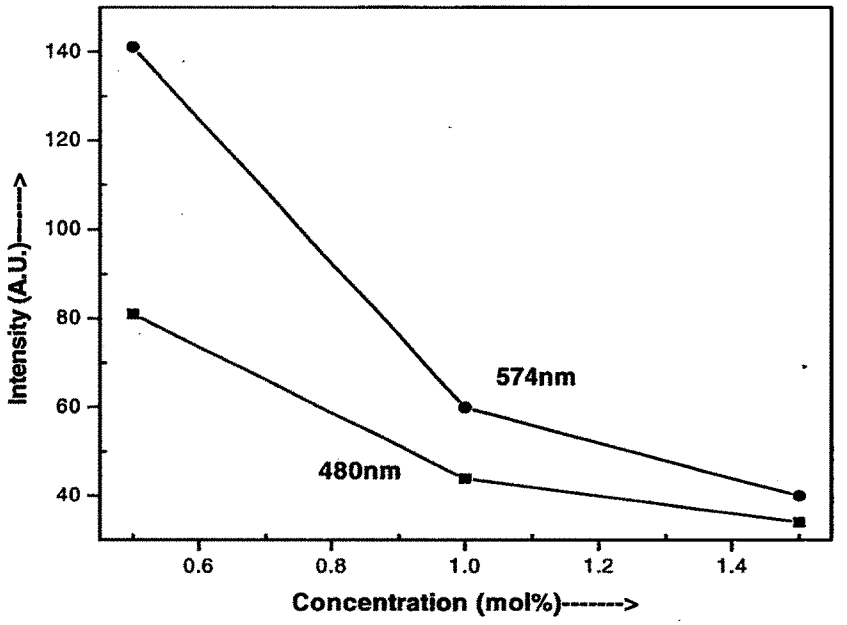

Figure-13 Variation of concentration with intensity at different wavelengths for the emission spectra.

On doping dysprosium we found that the visible emission from the nanocrsytal was predominantly yellow, from the $^4F_{9/2} \rightarrow {}^6H_{13/2}$ transition, centered at approximately 574nm. The emission spectra for all the concentrations of dysprosium (0.5, 1.0 and 1.5mol%) can be seen in the figure-12. This visible transition of dysprosium in the yellow region makes it an important material for technological applications, which require yellow light as emission. The visible spectra also consist of lines in the blue-green region at around 481nm and 490nm. These may be assigned to the transitions from $^4F_{9/2} \rightarrow {}^4H_{15/2}$. When the dominating lines are from the $^6H_{13/2}$ (574nm) transitions, then in this condition $\Delta J = 2$, so it is hypersensitive transition, hence we can say that the host lattice is hypersensitive [1]. Similar results were also observed for the Eu^{3+} which had a dominant $^5D_0 \rightarrow {}^7F_2$ transition, which is also a hypersensitive transition. No other higher transitions of Dysprosium were observed in the red and near IR region even at different mol% of doping. The photoluminescence spectra shows that it can be used to tune the emission color with different mol% of the Dysprosium. The emission spectrum for the host has a broad band due to Ce^{4+}-O^{2-} CT emission and it covers all the Dy^{3+} emission up to 600nm. It is also observed that the Dy^{3+} emission lines at 480nm are overlapped by the host emission and the lines at 574nm appear weak. On increasing the dysprosium concentration we found that the relative intensity of the host and as well as that of the Dy^{3+} emission decreases. The relative fall in the intensity of the Dy^{3+} emission at 574nm is much steeper than that of 480nm for the host, seen in the figure-13.

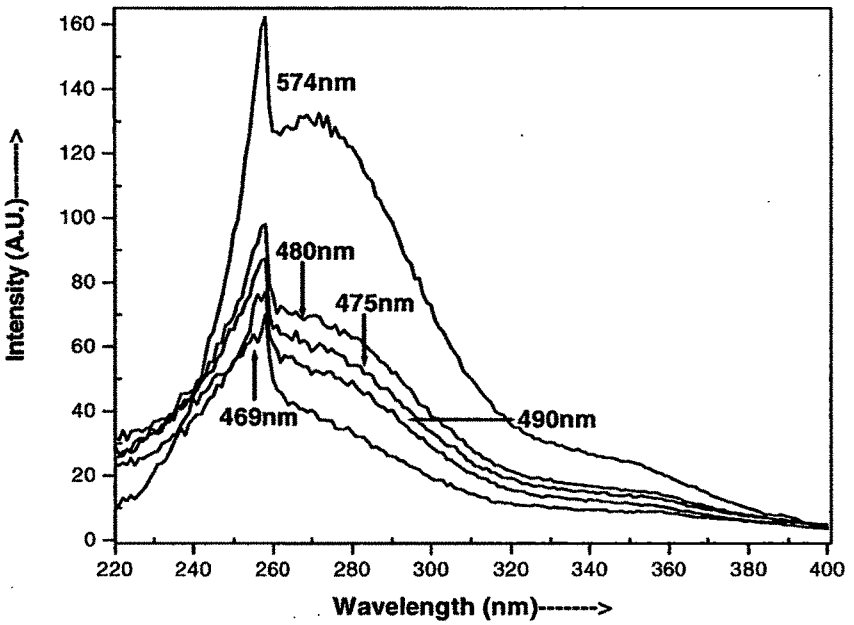

Figure-14 Photoluminescence excitation spectra of the $Sr_2CeO_4:Dy^{3+}$ (0.5mol%) monitored at different wavelengths.

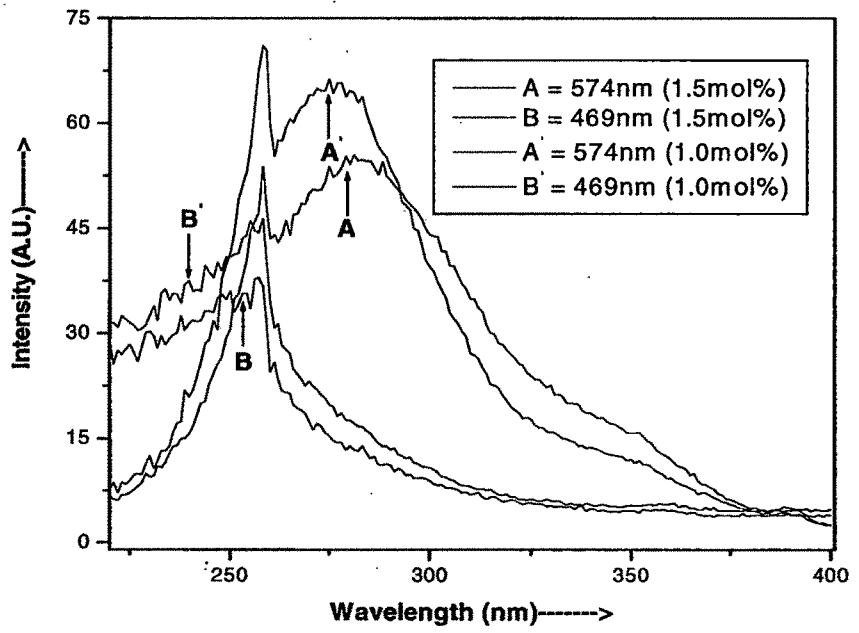

Figure-15 Photoluminescence excitation spectra of the $Sr_2CeO_4:Dy^{3+}$ (1.0 & 1.5mol%) monitored at different wavelengths.

The excitation spectra for all the samples are shown in figure-14, 15 (0.5, 1.0 and 1.5mol%) monitored with 574nm of the Dy^{3+} ion and the 469nm of the Sr_2CeO_4 host. The excitation spectrum has a strong absorption band with a maximum at 258nm (sharp peak) and a broad band at around 280nm (when monitored with 574nm). This is in lieu with the results of the excitation spectra of the host due to the two different bond lengths in the Ce-O [6]. The f-f transition lines of the trivalent Dysprosium are not observed due to their weak intensity relative to that of the host. As we observe from Figure-14 and 15 that under two different monitoring wavelengths, the excitation spectra showed difference in the shape of the spectra. When monitored with 469nm wavelength, the peak is at 258nm and then it falls steeply, whereas it has additional peak at around ~ 280nm. We are at variance with the results presented by He et al. [9], they showed that there is absolutely no difference while monitoring it with 472nm and 570nm.

The Sr_2CeO_4 doped with different concentrations of terbium was also studied. But the energy levels of the terbium does not match with that of the Sr_2CeO_4 hence the doping totally quenched the luminescence. The PL emission as well as excitation spectra don't show any luminescence of the terbium doped samples, this is in line with the results observed for the terbium by Nag et al [8].

5.4.4 CIE coordinates

The CIE coordinates for the Photoluminescence spectra of the doped samarium with 0.5mol% concentration are x = 0.21 and y = 0.24. These measurements were calculated by equidistant-wavelength method and have been elaborated in chapter two of this thesis. The given sample and then calculating the color coordinates x and y. The values of the CIE clearly suggest that on doping the host with samarium, the white light emission can be achieved from a single host compound rather than the mixing of three color phosphors (red, green and blue). This property of the synthesized phosphor makes it suitable and predicts its use in various display devices. Near white emission of $Sr_2CeO_4:Sm^{3+}$ is due to the coexistence of Ce^{4+}-O^{2-} charge transfer emission and the $^4G_{5/2} \rightarrow {}^6H_J$ (J = 5/2, 7/2) Sm^{3+} transitions.

CIE co-ordinates	CIE 1931		CIE 1960		CIE 1976	
Samarium Mole %	x	y	u	v	u′	v′
0.03125	0.166	0.260	0.114	0.269	0.114	0.404
0.125	0.177	0.249	0.126	0.265	0.126	0.398
0.25	0.193	0.252	0.136	0.268	0.136	0.402
0.5	0.216	0.243	0.157	0.265	0.157	0.398
1.0	0.198	0.211	0.154	0.246	0.154	0.370
1.5	0.194	0.206	0.153	0.243	0.153	0.365
2.0	0.214	0.223	0.163	0.255	0.163	0.382

Table-3 The values of CIE coordinates for the Samarium doped Sr_2CeO_4.

CIE Co-ordinates	CIE 1931		CIE 1960		CIE 1976	
Dysprosium Mole %	x	y	u	v	u′	v′
0.5	0.2	0.255	0.157	0.272	0.157	0.408
1.0	0.2	0.255	0.159	0.272	0.159	0.409
1.5	0.2	0.293	0.159	0.291	0.159	0.437

Table-4 Shows the values of CIE coordinates for the Dysprosium doped sample

On dysprosium doping of Sr_2CeO_4 (0.5, 1.0 and 1.5mol%) it was found to be varying by x = 0.22, y = 0.25 to x = 0.24, y = 0.29 for 0.5mol% to 1.5mol%. The depiction of these on the CIE 1931 and CIE 1976 have been shown.

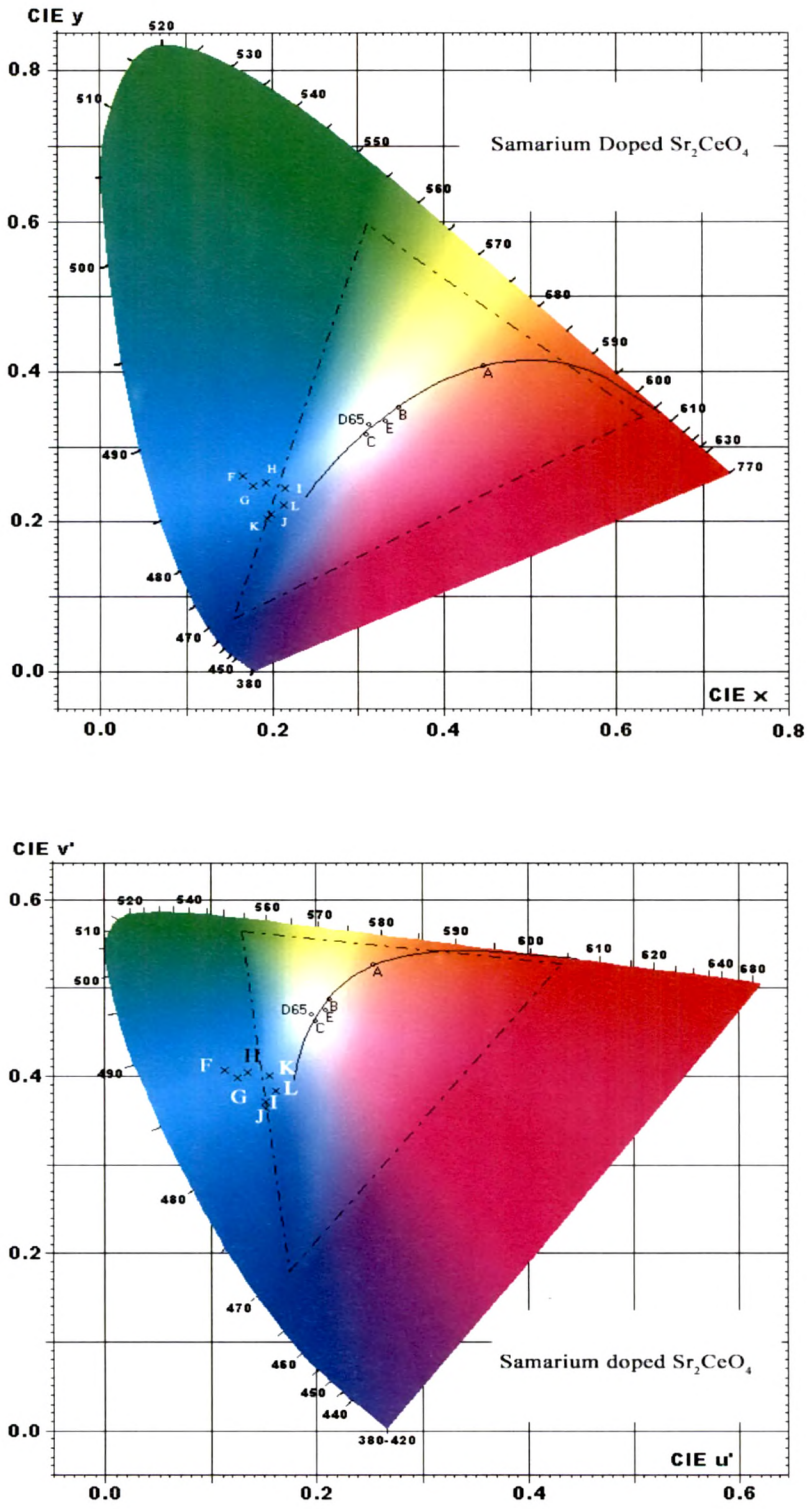

CIE Coordinates depicted on CIE 1931 and CIE 1976 (Where F=0.03125, G=0.125, H=0.25, I=0.5, J=1.0, K=1.5, L=2.0mol% of Samarium doped Sr_2CeO_4).

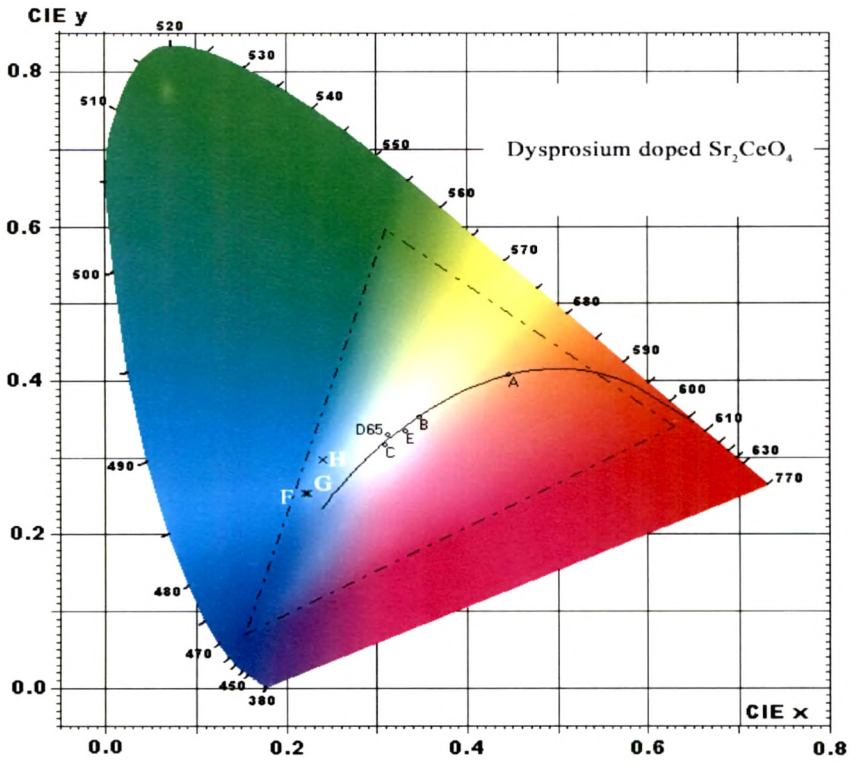

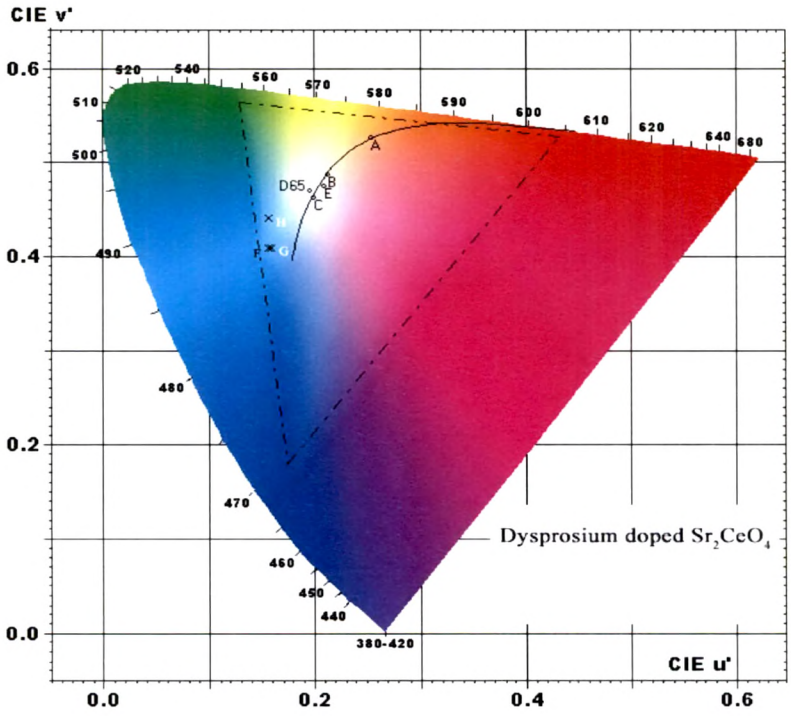

CIE Coordinates depicted on CIE 1931 and CIE 1976 (Where F=0.5, G=1.0, H=1.5mol% of Dysprosium doped Sr_2CeO_4)

5 Conclusions

The main conclusions that can be drawn by studying the effect of different rare pearth doping on the luminescence properties of the Sr_2CeO_4 are as follows:

1. The present study shows the successful synthesis of the Sr_2CeO_4 compound by the sol-gel route with the different rare earth dopants.
2. The luminescence arises from the charge transfer mechanism in the host compound. The energy transfer also occurs in between the host and the samarium and dysprosium dopant.
3. It was observed that there was no emission when terbium was doped into the host Sr_2CeO_4, so much so that the emission of the host also quenched.
4. The good luminescent properties, with the efficient white light emission from the Sr_2CeO_4 samarium doped compound were also observed.
5. The dysprosium sample also shows white light emission at higher concentrations.

References

1. G. Blasse, B.C. Grabmaeir, Luminescent Materials, Springer Verlag, Berlin, (**1994**).
2. S. Shionoya, W. Yen, Phosphor Handbook, CRC Press, Boca Raton, (**1999**).
3. W.B. Smith, R.C. Powell, Journal of Chemical Physics, 76, (2), (**1992**), 854-859.
4. H. Lina, X.Y. Wang, L. Lin, D.L. Yang, T.K. Xu, J.Y. Yu, E.Y.B. Pun, Journal of Luminescence, 116, (**2006**), 139–144.
5. E. De la Rosa, L.A. Diaz-Torres, P. Salas, R. A. Rodríguez, C. Angeles, Nanophotonic Materials, edited by David L. Andrews, Guozhong Z. Cao, Zeno Gaburro, Proc. of SPIE, 5510, SPIE, Bellingham, WA, (**2004**).
6. E. Danielson, M. Devenney, D. Giaquinta, J.H. Golden, R.C. Haushalter, W. McFarland, D.M. Poojary, C.M. Reaves, W. Henry Weinberg, X.D. Wu, Science, 279, (**1998**), 837.
7. R. Ghildiyal, P. Page, K.V.R. Murthy, Journal of Luminescence, 124, (**2007**), 217–220.
8. A. Nag, T.R.N. Kutty, Journal of Materials Chemistry, 13, (**2003**), 370-376.
9. X. He, W. Li, Q. Zhou, Materials Science and Engineering-B,134, (**2006**), 59-62.
10. S. Shi, J. Li, J. Zhou, Materials Science Forum, 475-479, (**2005**), 1181-1184.
11. S. Fujihara, M. Oikawa, Journal of Applied Physics, 95, (12), (**2004**), 8002-8006.
12. M. Oikawa, S. Fujihara, Journal of Solid state chemistry, 178, (**2005**), 2036-2041.
13. M. Oikawa, S. Fujihara, Journal of The Europium Ceramic Society, 25, (**2004**), 2921-2924.
14. E.D. La Roza-Cruz, L.A. Diaz-Torres, P. Salas, R.A. Rodriguez, G.A. Kumar, M.A. Meneses, J.F. Mosino, J.M. Hernandez, O. Barbosa Garcia, Journal of Applied Physics, 94 (**2003**), 3509.
15. F. Vetrone, J. Boyer, J.A. Capobianco, A. Speghini, M. Bettinelli, Nanotechnology, 15, (**2004**), 75-81.

16. A. Huignard, T. Gacoin, J.P. Pierre, Chem. Mater., 12, (**2000**), 1090.